

Non-trivial attenuation of geometric frustration by discretization of the degrees of freedom: A study of a Potts-like frustrated spin system.

Snir Meiri and Efi Efrati*

Department of Physics of Complex Systems, Weizmann Institute of Science, Rehovot 76100, Israel

(Dated: March 11, 2022)

The resolution of geometric frustration in systems with continuous degrees of freedom (DOF) often involves long-range cooperative response and super-extensive energy scaling. In contrast, frustrated Ising-like spin systems show only a local and uniform resolution of the frustration. In this work we bridge between these two extremes by studying a frustrated N -state Potts-like spin model and varying N . The expected cooperative response, observed for large N , is strongly attenuated as N is reduced. Moderate N values show unique phases that result from the discrete compatibility conditions.

Geometric frustration arises whenever the short-range interactions between the constituents of a system favor the formation of local motifs that are incompatible with long range propagation in the ambient space geometry or topology. Frustrated assemblies occur naturally in a wide variety of systems from spin systems [1–4], to liquid-crystals [5–8], to twisted molecular crystals [9, 10] and biological fibrillar assemblies [11].

As the locally favored arrangement of the constituents cannot be realized, any finite assembly must exhibit some compromise of these locally favored tendencies. In some cases, such as the Ising anti-ferromagnet on triangular lattice, this compromise could be made uniform. Consequently the energy associated with this compromise will grow extensively, proportionally to the number of constituents. Such frustration was recently termed non-cumulative [12], in contrast with systems exhibiting cumulative frustration, such as the frustrated XY-model [13]. In the latter model the optimal compromise in a single triangular facet precludes repeating the same compromise verbatim in the adjacent facets. As a result the energy associated with the compromise in systems exhibiting cumulative frustration grows super-extensively, and the ground-state shows long range cooperativity and depends on global properties of the systems such as its aspect ratio and its spatial extent. The super-extensive energy scaling and its dependence on global parameters may lead to growth arrest [14], formation of filamentous structures [15, 16], and give rise to exotic response properties [17, 18]. Naturally, the super-extensive energy scaling does not persist in the thermodynamic limit and only applies to finite systems. Different types of geometric frustration may exhibit distinct mechanisms for frustration saturation for large systems, and in particular could result in infinite bulks of extensive energy, or growth arrest along one or a few dimensions [6]. The classification of frustration to cumulative or non-cumulative in continuous systems was recently shown to be encoded in the compatibility conditions that relate the fields describing the local geometric tendencies of the matter and their spatial derivatives to the properties of the ambient space [12]. Moreover, the form of the compatibility conditions

allows to predict the super-extensive energy scaling exponent without explicitly solving the ground-state of the system. The structure of the compatibility conditions in systems possessing discrete DOF is different, and thus the continuous analysis [12] cannot be simply applied to such systems.

Considering moderately sized systems [19] with discrete DOF we encounter very different limiting behaviors: when the discrete DOF may assume a very large number of states, N , one expects to recover the continuous behavior and allow for cumulative frustration. However, it was recently shown that for low N values the resolution of the frustration is local and the frustration saturates at the level of a single or a few facets [20]. The present work aims to understand this discrepancy by filling in the gap between these two distinct and limiting behaviors.

We consider a frustrated Potts-like spin model. The basic components of the model, located on the vertices of a triangular lattice, are Potts spins that can be oriented along N equally-spaced orientations in the plane. The interactions of the spins are set to favor slight misalignment according to the following Hamiltonian:

$$\mathcal{H} = \frac{1}{2} \sum_{\text{facets}} K_1 \Psi_1^2 + K_3 (\Psi_2 - b_0)^2. \quad (1)$$

where the auxiliary variables Ψ_i are defined using the notations in Figure 1 (a) as:

$$\begin{aligned} \Psi_1 &= -\frac{\theta_2 - \theta_1}{l} \sin(\bar{\theta}) \pm \frac{2\theta_3 - \theta_2 - \theta_1}{\sqrt{3}l} \cos(\bar{\theta}), \\ \Psi_2 &= \frac{\theta_2 - \theta_1}{l} \cos(\bar{\theta}) \pm \frac{2\theta_3 - \theta_2 - \theta_1}{\sqrt{3}l} \sin(\bar{\theta}). \end{aligned} \quad (2)$$

In the limit $N \rightarrow \infty$ this model recovers the recently introduced frustrated XY-spin model [13] exhibiting cumulative frustration. In this limit the spin texture is interpreted as a director field and Ψ_1 and Ψ_2 are identified with the director's splay and bend fields respectively. For finite N values Ψ_1 and Ψ_2 may only assume a finite collection of states, which is further reduced by the discrete compatibility conditions. For more details regarding the manner in which this model is related to planar bent-core

liquid-crystals and regarding the response in the case of the frustrated XY-spin model see [13].

In order to probe the effects of discrete response modes on the frustrated conformations of minimal energy, the ground-state of the system was approached numerically. Due to the highly coupled nature of the problem the stochastic sampling of individual spins proved inefficient, and at each step a pair of edge-sharing spins were sampled. The numerical process included two rounds each comprised of a simulated annealing step combined with a global step that probed the energetic benefit associated with the rigid rotation of domains of finite size in the system. For more details see supplementary material. The chosen parameters are $K_1 = K_3 = 2$, edge length in the lattice of $l = 2$ and preferred misalignment of $b_0 = 0.015$. Free boundary conditions were used throughout the optimization process.

The spins of a given triangle in the lattice are ordered according to panel (a) of Fig. 1 and their states are expressed as $[m_1, m_2, m_3]$, where m_i are positive integers between 1 and N corresponding to their orientations. Note that in throughout this work the local orientations were bounded away from both 0 and 2π , thus the periodicity of the angular variable did not come into play. In order to focus on the spatial gradients in the orientation we identify the minimal orientation value in each facet, $\min(m_i) = m$, and express the facet orientation as $[m+a, m+b, m+c]$ with a, b and c non-negative integers, at least one of which is zero. Each type of spatial gradient about m corresponds to a specific triplet (a, b, c) and is color-coded consistently throughout this manuscript.

Considering a single triangular facet, and the misalignment b_0 , it is not always favorable to form any gradient of the orientations. The state $[m, m, m]$ represents the trivial constant solution and the state $[m, m, m+1]$ represents the smallest possible deviation from it (along with its permutations). Given a certain value of b_0 , it might be unfavorable to form any type of non-trivial solution as the lowest possible deviation of the orientations is too large. One can treat N , the granularity of the Potts model, as a variable in order to find the threshold N_t at which a non-trivial solution becomes energetically favorable. The energetic cost of the trivial solution is $e = b_0^2$. The energetic cost of the smallest deviation from it reads:

$$e = b_0^2 + \frac{4\pi^2}{3N^2} - \frac{4\pi b_0}{\sqrt{3}N} \sin\left[\left(m + \frac{1}{3}\right) \frac{2\pi}{N}\right]. \quad (3)$$

This energy is favorable whenever:

$$N > \frac{\pi}{\sqrt{3}b_0 \sin\left[\left(m + \frac{1}{3}\right) \frac{2\pi}{N}\right]}. \quad (4)$$

As we are interested in the threshold for incorporating gradients, we substitute for largest possible denominator, obtained for $\left(m + \frac{1}{3}\right) \frac{2\pi}{N} = \frac{\pi}{2}$. Assuming this value is approximately achievable and setting $b_0 = 0.015$ we obtain: $N_t > 120.91$.

Panel (c) of Fig. 1 shows the optimal energy of a single facet vs. N for several gradient types. One can see that the threshold at which the trivial solution, marked with a dashed line, ceases being the most favorable reads $N_t = 121$. Incorporating a deviation from a given orientation, m , may exclude repeating the same gradient type with the same m value in its vicinity. As the energy depends on the value of m the energetic cost of a uniform gradient in the system may vary spatially. The minimized conformations in the case of a marginal granularity of $N = 124$ is shown in panel (d). The uniform gradient causes the value of m to vary spatially leading the gradient orientation to deviate away from the local average orientation and thus contribute to Ψ_1 rather than Ψ_2 . Consequently, after incorporating nine lines of a vertical gradient, the trivial solution becomes most favorable. In general, for marginal values of N the non-trivial solutions may be supported only by small domains up to a finite size. Further increasing the size of the domain incorporates only domains of trivial solution rendering the energetic signature of the non-trivial regions less distinguishable, as can be seen in panel (e).

As the granularity of the orientation of the spins is reduced, by increasing N , more complex response modes are incorporated into the ground-state. While marginal values of N only display uniform gradient ground-states, i.e. the entire solution is comprised of a single gradient type $[m + a, m + b, m + c]$, for higher values of N non-uniform responses appear.

Figure 2 displays representative samples of the ground-state solutions for $N = 356$ depicting the transition between gradient types as the domain size is increased. From panel (c) of figure 1 we deduce that for $N = 365$ the gradient $[m + 1, m, m + 2]$ is associated with the minimal energy for a single triangle, while the gradient $[m, m, m + 1]$ is associated with the next lowest energy. Indeed, the ground-state of the smallest domain in panel (a) of figure 2 displays only a single gradient $[m + 1, m, m + 2]$. Moreover, as depicted in panel (e) of figure 2, the energy associated with the uniform gradient $[m + 1, m, m + 2]$ increases very fast with system size, while the energy associated with the uniform gradient $[m, m, m + 1]$ grows at a much slower rate. Consequently, for larger systems we expect the gradient type $[m, m, m + 1]$ to dominate the ground-state solution, as seen in panel (c). Note, that the transition is not abrupt, and that the system succeeds in further lowering the elastic energy by incorporating additional gradient types. This behaviour demonstrates the global aspects of cumulative geometric frustration, as the optimal solutions for larger domain may be fundamentally different from the solutions for smaller domains.

As the value of N is further increased large domains display more intricate ground-states. Figure 3 displays the ground-state for three domain sizes for $N = 446$. Panel (a) shows a relatively small domain in which

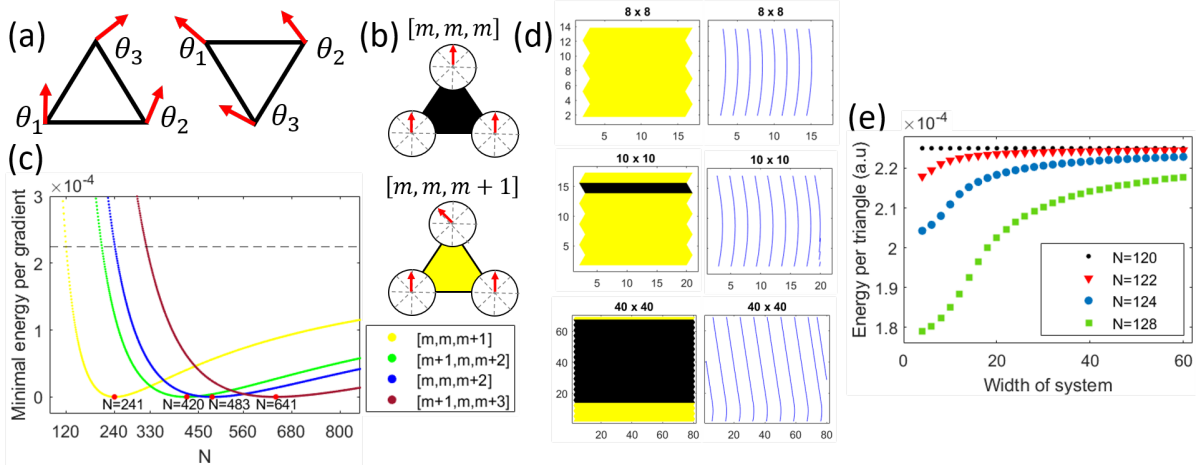


FIG. 1. (a) Notations of vertices of upright (left) and up-side-down (right) triangles. (b) Color coding of two possible conformations of the spins. The state-key on top is defined such that each entry represents a state of a spin according to the notations in (a). m is any integer between 1 and N where N is the number of states in the Potts model. (c) The minimal energy of a single triangle in a given conformation type for different N values. The N at which this minimal value is attained is marked. (d) Resulting minimal conformations for lattices of 8×8 , 10×10 and 40×40 sites per edge in the case of $N = 124$. Color coding is according to (b). (e) Energy per triangle vs. the width of the system (number of sites per edge) for different values of N near the cumulative-non-cumulative transition.

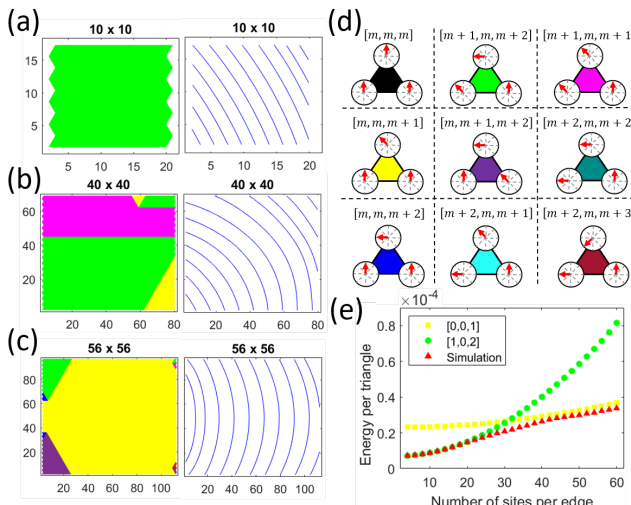


FIG. 2. Results for $N = 356$. (a) Resulting minimal conformations for lattices of 10×10 , 40×40 , 42×42 and 56×56 sites per edge. Color coding is according to (b). (c) Energy per triangle vs. the number of sites per edge in isotropically growing lattices. The resulting conformations from the simulation marked in red triangles are shown together with the minimal energies per triangle in lattices of a single conformation where $[m, m, m+1]$ and $[m+1, m, m+2]$ are marked in yellow squares and green circles, respectively.

the ground-state is given by the uniform gradient $[m+1, m, m+2]$, as predicted in Figure 2 (c) for a single triangle. Note, however, that while the gradient is uniform the energy is not; the local energy also depends on the relative orientation between the direction of the gradient

and the average local orientation given by m . Panel (e) shows the dependence of the energy of a single triangular facet of nine gradient types on the local value of m . The energetically favorable gradient type for a certain m value may be succeeded by another gradient type as m is varied. In the constant gradient solution displayed in Figure 3 (a) the optimal m value is obtained along one of diagonals of the domain. Away from this diagonal m varies, leading to the strain energy buildup in the top-left and bottom-right corners of the domain. Figure 3 (b) shows that as the domain size is increased the growing strain is screened by incorporating different gradient types in these energetically unfavorable regions, namely $[m, m, m+2]$ and $[m+2, m, m+2]$. Note, however, that the discrete compatibility conditions preclude the gradient type $[m, m, m+2]$ at the bottom right from having a horizontal or upper-right diagonal interfaces with the underlying $[m+1, m, m+2]$ gradient. Consequently, it must be buffered by an additional gradient type, $[m, m, m+1]$, that bridges between the incompatible gradients. While the buffering gradient $[m, m, m+1]$ is less energetically favorable, its presence is necessitated by the discrete compatibility conditions. In the upper-left corner of Figure 3 (b) we similarly observe the incorporation of a buffering gradient $[m+2, m, m+3]$ to bridge between two incompatible gradients.

Panel (c) in Figure 3 depicts a further increase in domain size and the appearance of more intricate texture. A new gradient type $[m+1, m, m+1]$ (marked by the pink domain) is incorporated near the top-left portion of the domain to reduce the local stain. This gradient type, while allowing horizontal interfaces with the underlying

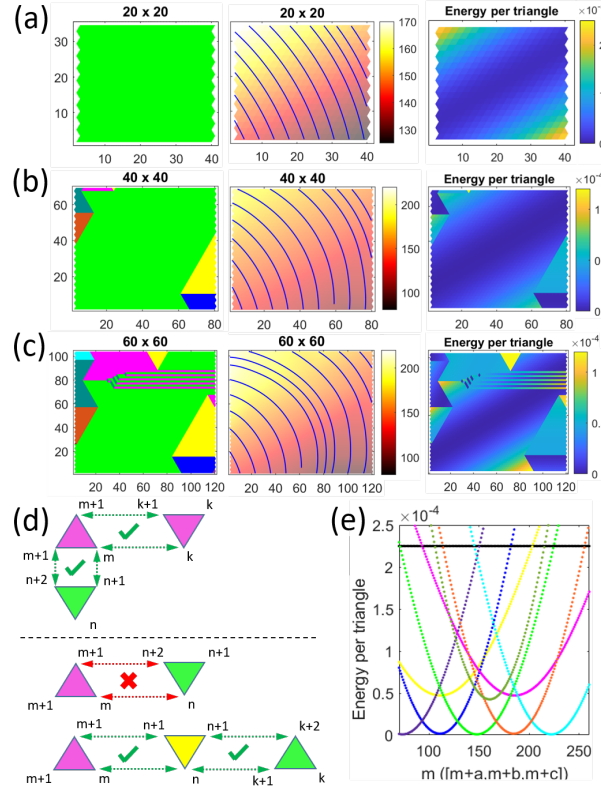


FIG. 3. Results for $N = 446$. (a)-(c) Resulting minimal conformations for lattices of (a) 20×20 , (b) 40×40 and (c) 60×60 sites per edge. Color coding is according to panel (b) of figure 2. Each triplet shows gradient types, interpolated streamlines along with m value and energy per site (left to right). Notice different color-bar scales. (d) Allowed horizontal and vertical transitions between triangles of the pink and green types. (e) Energy per a single triangle of a conformation $[m+a, m+b, m+c]$ vs. m in that notation. The color coding is also according to panel (b) of figure 2.

$[m+1, m, m+2]$ gradient (marked in green), cannot share any diagonal interface with it. Consequently here too a buffering gradient is required. Growing the buffering gradient $[m, m, m+1]$ (marked in yellow) along the entire incompatible interface is prohibitively energetically costly. As a result the bottom region of the (pink) gradient $[m+1, m, m+1]$ must extend all the way to the boundary of the domain. This gives rise to the (pink) striped pattern in the upper-half of panel (c) in Figure 3. These stripes, while energetically unfavorable compared to the underlying gradient, are required by the compatibility conditions to reach a boundary. Such topological transitions are expected to become more prevalent as the energy associated with the buffering gradient domains becomes exceedingly large.

Considering the energy scaling with system size we observe the expected transition from a uniform resolution of the frustration at low N values to a highly cooperative ground-states exhibiting a super-extensive energy

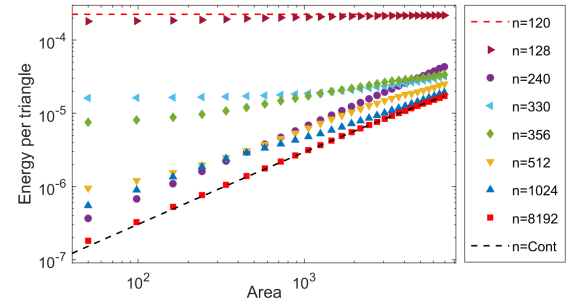


FIG. 4. Logarithmic plot of the energy per triangle of the ground-states resulting from the simulation vs. the area of isotropic domains for different directions granularity values, N . The black dashed line (bottom) shows the results in the case of the continuous XY-spins, as was presented in [13].

scaling at large N values. Large enough N values recover quantitatively the behavior of the corresponding continuous frustrated XY-spin system [13]: $E/M \propto M$. Figure 4 shows that for $N = 8192$ the system follows closely the super-extensive energy scaling of the continuous case, while the system at $N = 120$ follows an extensive energy scaling. The transition between these two limiting behaviors is, however, non-monotonic. For example, while $N = 128$ follows closely the extensive scaling, $N = 240$ displays a super-extensive scaling quite similar to the continuous case, and $N = 330$ again shows only small deviations from an extensive behavior. Naïvely, one would expect that as N is increased, more refined gradients could be constructed to better approximate the continuous case; this is indeed the case for large N values. For moderate N -values, however, “resonant”-like values of N could approximate the attempted gradient b_0 almost perfectly, while nearby increased values such as $N + 1$ will not perform as well. These discrete effects, most prominently manifest for moderate N -values also affect the compatibility conditions and the rate at which the energy of a given gradient varies as m is varied.

The frustrated N-state Potts-like spin model presented here allows us to bridge the gap between the cumulative frustration of the frustrated XY-model, and the non-cumulative frustration of the Ising anti-ferromagnet on triangular lattice. Up until $N_t = 121$ all the spins in the ground-state are co-aligned, and the ground-state energy is extensive. The threshold value N_t is inversely proportional to the relatively small strength of the frustration $b_0 \ll 1$. While increasing b_0 might lower N_t , it also decreases the length-scale associated with the geometric frustration and thus diminishes the domain size at which frustration saturation is met. Eventually, when the geometric length-scale associated with the frustration becomes shorter than a single unit cell, no characteristics of the cumulative frustration will remain [12]. Thus, in order to see the effects of cumulative frustration over do-

main sizes consisting at least a few dozens sites, the value of the geometric frustration is required to be small.

For large values of N the cumulative frustration behavior of the continuum limit is recovered and the granularity of the DOF does not play a significant role in shaping the ground-state. However, for moderate values of N , while we observe cumulative frustration and a highly cooperative ground-state, the discrete nature of the DOF leads to qualitatively different ground-states and exotic response properties that are not observed in the continuous case. These include the formation of striped patterns and the appearance of buffering moderate energy regions that facilitate the incorporation of low energy domains whose incorporation is otherwise precluded by the discrete matching rules. These motifs are unique to the discrete-frustrated-spin system and have no analogue in the continuous frustrated XY-model.

* efi.efrati@weizmann.ac.il

- [1] G. H. Wannier. Antiferromagnetism. The Triangular Ising Net. *Physical Review*, 79(2):357–364, July 1950.
- [2] S. Teitel and C. Jayaprakash. Josephson-Junction Arrays in Transverse Magnetic Fields. *Physical Review Letters*, 51(21):1999–2002, November 1983.
- [3] Thomas C. Halsey. Josephson-junction arrays in transverse magnetic fields: Ground states and critical currents. *Physical Review B*, 31(9):5728–5745, May 1985.
- [4] Martijn Lankhorst, Alexander Brinkman, Hans Hilgenkamp, Nicola Poccia, and Alexander Golubov. Annealed Low Energy States in Frustrated Large Square Josephson Junction Arrays. *Condensed Matter*, 3(2):19, June 2018.
- [5] Robert B. Meyer. Structural Problems in Liquid Crystal Physics. In Balian R. and Weill G., editor, *Molecular Fluids, Les Houches Lectures, 1973*. Routledge, 1976.
- [6] Michael F. Hagan and Gregory M. Grason. Equilibrium mechanisms of self-limiting assembly. *Reviews of Modern Physics*, 93(2):025008, June 2021.
- [7] Idan Niv and Efi Efrati. Geometric frustration and compatibility conditions for two-dimensional director fields. *Soft Matter*, 14(3):424–431, January 2018.
- [8] Jonathan V. Selinger. Director Deformations, Geometric Frustration, and Modulated Phases in Liquid Crystals. *Annual Review of Condensed Matter Physics*, 13(1):null, 2022.
- [9] Asaf Haddad, Hillel Aharoni, Eran Sharon, Alexander G. Shtukenberg, Bart Kahr, and Efi Efrati. Twist renormalization in molecular crystals driven by geometric frustration. *Soft Matter*, 15(1):116–126, 2019.
- [10] Chao Li, Alexander G. Shtukenberg, Leslie Vogt-Maranto, Efi Efrati, Paolo Raiteri, Julian D. Gale, Andrew L. Rohl, and Bart Kahr. Why Are Some Crystals Straight? *The Journal of Physical Chemistry C*, 124(28):15616–15624, July 2020.
- [11] Aidan I. Brown, Laurent Kreplak, and Andrew D. Rutenberg. An equilibrium double-twist model for the radial structure of collagen fibrils. *Soft Matter*, 10(42):8500–8511, 2014.
- [12] Snir Meiri and Efi Efrati. Cumulative geometric frustration in physical assemblies. *Physical Review E*, 104(5):054601, November 2021.
- [13] Snir Meiri and Efi Efrati. Cumulative geometric frustration and superextensive energy scaling in a non-linear classical XY-spin model. *Physical Review E*, 105(2):024703, February 2022.
- [14] Botond Tyukodi, Farzaneh Mohajerani, Douglas M. Hall, Gregory M. Grason, and Michael F. Hagan. Thermodynamic size control in curvature-frustrated tubules: Self-limitation with open boundaries. *arXiv:2109.01174 [cond-mat]*, September 2021.
- [15] Guangnan Meng, Jayson Paulose, David R. Nelson, and Vinothan N. Manoharan. Elastic Instability of a Crystal Growing on a Curved Surface. *Science*, 343(6171):634–637, February 2014.
- [16] Martin Lenz and Thomas A. Witten. Geometrical frustration yields fibre formation in self-assembly. *Nature Physics*, 13(11):1100–1104, November 2017.
- [17] Kai Sun and Xiaoming Mao. Fractional Excitations in Non-Euclidean Elastic Plates. *Physical Review Letters*, 127(9):098001, 2021.
- [18] Ido Levin and Eran Sharon. Anomalously Soft Non-Euclidean Springs. *Physical Review Letters*, 116(3):035502, 2016.
- [19] smaller than the geometric scale associated with the frustration.
- [20] Pierre Ronceray and Bruno Le Floch. Range of geometrical frustration in lattice spin models. *Physical Review E*, 100(5):052150, November 2019.

METHOD

The numerical scheme employs two iterations of simulated annealing. The strong energy coupling between edge sharing facets results in significant energy barriers. Consequently, single spin variations are generally unfavorable even in high energy configurations. To circumvent this difficulty at every time-step the value of an edge-sharing spin pair is probed.

Spin orientation values are varied by single-steps, i.e. for a spin at the state m , the scheme only considers the states $m - 1, m, m + 1$. Throughout the process all spin orientations are far from 0 and 2π , thus we need not address comparing spin values across the orientation discontinuity. For every spin pair chosen, each of the nine possible states is examined and its energy variation, Δ_i , is computed. The resulting state, i , is drawn from the probability $e^{-\frac{\Delta_i}{T}} / \sum_{k=1}^9 e^{-\frac{\Delta_k}{T}}$, where T is the temperature at the step. To overcome energy barriers in the rugged energetic landscape of the system the simulated annealing stages are followed by the exploration of more favorable states arrived to by global transformations involving many spins. In these transformations all the spins in the system (or in a large domains near the boundary) are simultaneously rotated by the same value. This global stage is followed by another annealing stage. The results presented in this work were obtained by repeating

such a cycle twice.

Each cycle starts with an annealing stage separated to a faster stage at which the temperature is lowered linearly from $T = 2$ to $T = 0.3$ at equal decrements over the number of steps given by $n_{Iter,1} = n_{Sites} * \max(400, N)$, where as in the main text N denotes the spin's number of states. At the second stage of annealing the rate is slowed and the temperature reduction proceeds over $n_{Iter,2} = n_{Sites} * \max(900, 2.25 * N)$ time-steps. A single step before reaching vanishing temperature the annealing is stopped and global transformations are explored, and

accepted if they lead to a reduction in energy. The global transformations include varying all spin values by uniformly rotating them by $-16 \leq \delta \leq 16$ steps (For low N values this was reduced to $-N/20 \leq \delta \leq N/20$). In addition sectioning the system by a single horizontal, diagonal or vertical line and assigning distinct uniform rotations in the two domains is explored. A third phase of annealing is performed next, consisting of $n_{Iter,3} = \lfloor \frac{n_{Iter,2}}{3} \rfloor$ steps with temperature decrements of $dT_3 = \frac{T_{Ini,3}}{n_{Iter,2}+1}$, where $T_{Ini,3}$ is the temperature at the beginning of the stage, which coincides with the temperature of the last step of the preceding annealing stage.